MCB
Journals.ASM.org

Loss of Osteoblast Runx3 Produces Severe Congenital Osteopenia

Omri Bauer,[a] Amnon Sharir,[a]* Ayako Kimura,[b]* Shay Hantisteanu,[a] Shu Takeda,[b]* Yoram Groner[a]

Department of Molecular Genetics, Weizmann Institute of Science, Rehovot, Israel[a]; Department of Orthopedics, Tokyo Medical and Dental University, Tokyo, Japan[b]

Congenital osteopenia is a bone demineralization condition that is associated with elevated fracture risk in human infants. Here we show that *Runx3*, like *Runx2*, is expressed in precommitted embryonic osteoblasts and that Runx3-deficient mice develop severe congenital osteopenia. Runx3-deficient osteoblast-specific (*Runx3*$^{fl/fl}$/*Col1α1*-cre), but not chondrocyte-specific (*Runx3*$^{fl/fl}$/*Col1α2*-cre), mice are osteopenic. This demonstrates that an osteoblastic cell-autonomous function of Runx3 is required for proper osteogenesis. Bone histomorphometry revealed that decreased osteoblast numbers and reduced mineral deposition capacity in Runx3-deficient mice cause this bone formation deficiency. Neonatal bone and cultured primary osteoblast analyses revealed a Runx3-deficiency-associated decrease in the number of active osteoblasts resulting from diminished proliferation and not from enhanced osteoblast apoptosis. These findings are supported by Runx3-null culture transcriptome analyses showing significant decreases in the levels of osteoblastic markers and increases in the levels of Notch signaling components. Thus, while Runx2 is mandatory for the osteoblastic lineage commitment, Runx3 is nonredundantly required for the proliferation of these precommitted cells, to generate adequate numbers of active osteoblasts. Human *RUNX3* resides on chromosome 1p36, a region that is associated with osteoporosis. Therefore, RUNX3 might also be involved in human bone mineralization.

Long bones in vertebrates are formed by endochondral ossification via a cartilage intermediate. Other parts of the skeleton, e.g., the flat bones of the skull, are formed via intramembranous ossification, involving the direct differentiation of mesenchymal cells to osteoblasts (OBLs). Osteogenesis depends on the development of bone-forming OBLs (osteoblastogenesis) and is the endpoint in both these processes (1). Osteoblastogenesis proceeds through the commitment of progenitor cells, their differentiation into pre-OBLs, and the final maturation into active OBLs (2). OBLs then differentiate through three major stages: cellular proliferation (mainly of early mesenchymal stem cells), matrix maturation, and mineral deposition (3). In mice, the first OBLs appear in the bone collar (perichondrium) on embryonic day 14 (E14) to E14.5. These cells then ride the invading vasculature and reach the inner calcified matrix around the hypertrophic chondrocytes, where they form the primary spongiosa (1, 4). Primary spongiosa OBLs form the bone trabeculae (i.e., the cancellous part), while bone collar OBLs give rise to the bone cortex (5).

Osteoblastogenesis is tightly controlled by signal transduction and gene expression regulation (3, 6). The runt domain transcription factor (TF) Runx2 is the osteogenic master regulator that hubs the majority of these processes by integrating signals from various developmental cues (7, 8). Thus, Runx2-null mice are completely devoid of OBLs and bones (9–11), and transgenic expression of Runx2 (12) or its two isoforms, Runx2-I and Runx2-II (13), in OBLs results in severe osteopenia and bone fragility due to the inhibition of OBL maturation. Interestingly, recent findings suggest that Runx2 is not required for precommitted OBL lineage cell generation, even though it is mandatory for progenitor cell commitment to the osteogenic lineage (14, 15). This indicates that as-yet-unidentified participants are involved in osteoblastogenesis proper.

Runx3 is another member of the mammalian runt domain TF family, which includes Runx1, Runx2, and Runx3 (16). These TFs bind DNA as heterodimers with the non-DNA-binding subunit core-binding factor β (Cbf-β), which is essential for their proper function (17). More recently, Cbf-β was implicated in bone and skeletal development (18–20). During mouse embryogenesis, *Runx3*, the evolutionary founder of the *Runx* gene family (21–23), is expressed in the peripheral nervous system, hematopoietic cells, skin appendages, teeth, and skeleton (24, 25). Accordingly, Runx3-null mice develop sensory limb ataxia (26) as well as airway and colon inflammation (27–29). Although the three *Runx* genes are expressed in the limb bud mesenchyme, their role in the formation of the cartilaginous anlagen of the skeleton is unclear (30). In contrast, Runx3 along with Runx2 are well-established key regulators of chondrogenesis (30, 31). Ablation of *Runx3*, which regulates early and late chondrocyte differentiation (32), leads to delayed chondrocyte maturation and vascular invasion in E15.5 Runx3-null embryos (33). On the other hand, Runx3 overexpression in chondrocytes results in ectopic mineralization of the mouse rib cage (31). Likewise, Runx2-null mice develop a plethora of chondrocyte maturation abnormalities (33–35), and mice deficient in both Runx2 and Runx3 lack mature chondrocytes (33), attesting to their cooperative function in this lineage. Thus, the emergence and homeostasis of bone-building chondrocytes

Received 30 August 2014 **Returned for modification** 7 October 2014
Accepted 30 December 2014

Accepted manuscript posted online 20 January 2015

Citation Bauer O, Sharir A, Kimura A, Hantisteanu S, Takeda S, Groner Y. 2015. Loss of osteoblast Runx3 produces severe congenital osteopenia. Mol Cell Biol 35:1097–1109. doi:10.1128/MCB.01106-14.

Address correspondence to Yoram Groner, Yoram.Groner@weizmann.ac.il.

* Present address: Amnon Sharir, Department of Orofacial Sciences, University of California at San Francisco, San Francisco, California, USA; Ayako Kimura, Department of Orthopedic Surgery, Tokyo Medical and Dental University, Tokyo, Japan; Shu Takeda, Department of Physiology and Cell Biology, Tokyo Medical and Dental University, Tokyo, Japan.

Supplemental material for this article may be found at http://dx.doi.org/10.1128/MCB.01106-14.

doi:10.1128/MCB.01106-14

and OBLs that share a common mesenchymal osteochondroprogenitor cell (6, 36) are regulated by both Runx family members.

While the central role of Runx2 in osteoblastogenesis is well established (6, 37), the function of Runx3 in this process remains obscure. Given the common OBL-chondrocyte progenitor and Runx3/Runx2 cooperation in chondrogenesis, we hypothesized that Runx3 could also be involved in osteoblastogenesis. Here we report that Runx3 functions in committed OBLs of the developing bone and that its loss leads to reduced numbers of active OBLs, resulting in diminished bone formation and severe congenital osteopenia. Of note, the human *RUNX3* gene resides on chromosome 1p36 (38), a region associated with low bone mineral density and osteoporosis (39–45). Thus, RUNX3 deficiency might also affect bone mineralization in humans and may constitute a risk factor for human osteopenia.

MATERIALS AND METHODS

Mice. Mouse strains used in this study include the previously described *Runx3* knockout (KO) (ICR background) (26), LoxP-flanked *Runx3* (*Runx3*$^{LoxP/LoxP}$) and *Runx3*$^{fl/fl}$/*Pgk*-cre (46), and *Runx2*$^{+/-}$ (11) mouse strains. *Runx3*$^{fl/fl}$/*Col1α1*-cre, *Runx3*$^{fl/fl}$/*Col1α2*-cre, and *Runx3*$^{fl/fl}$/*Osx1*-cre mice were generated by crossing *Runx3*$^{LoxP/LoxP}$ mice to *Col1α1*-cre (47), *Col1α2*-cre (48), and *Osx1*-cre (49) transgenic mice, respectively. Mice used in the experiments were 23-day-old (D23) females, unless stated otherwise. Histopathology was used to verify the absence of colitis in *Runx3* KO mice. The different cre-deleter mouse strains were of a mixed genetic background; hence, we used only gender-matching littermates as controls, to account for variation in bone parameters. Control mice were wild-type (WT) (*Runx3*$^{+/+}$) gender-matched littermate mice, unless indicated otherwise. All experiments were conducted according to protocols approved by the Institutional Animal Care and Use Committee of the Weizmann Institute of Science (permit numbers 01370311-2 and 00760108-2).

Alcian blue-alizarin red S staining. Mouse cadavers were deskinned, eviscerated, ethanol-acetone fixed, and stained with alcian blue and alizarin red S, as previously described (50). Stained cadavers were immersed in a 1% potassium hydroxide solution (in 20% glycerol) until complete clearing of soft tissue. Incubation times were empirically adjusted to the mouse developmental stage (embryonic or postnatal).

Micro-computed tomography. Femora were scanned with a high-resolution X-ray micro-computed tomography (μCT) system (eXplore Locus SP; General Electric, USA) with source settings at 80 kV and 80 μA. Sixteen-micrometer voxel-size images were analyzed with custom software (MicroView reconstruction version 5.2.2). Cortical and cancellous bone parameters were obtained from a fixed 0.5-mm (32 image slices) transverse section of the diaphysis (the long bone shaft; distally adjacent to the *trochanter tertius*) and the distal epiphysis (end part), respectively. A direct three-dimensional (3D) model was employed to determine the number, thickness, and separation of trabeculae as well as bone mineral density (BMD) and bone mineral content (BMC).

Whole-bone biomechanical testing. A 3-point bending assay was performed with an Instron material testing machine (model 3345), as described previously (51). Loading proceeded at a constant rate (2 mm/min) until bone fracture. Force-displacement data were collected with the system software (BlueHill) at 10 Hz. Tibial stiffness (S) was deduced from the slope of the load displacement plot, and the effective Young's modulus value (E) was calculated from the equation $E = S \cdot L^3/48 \cdot I$ (where S is bone stiffness, L is support span, and I is the moment of inertia around the bending axis, determined by μCT at the area of fracture).

RNA *in situ* hybridization (RISH). Radioactive *in situ* hybridization on paraffin sections was performed according to standard procedures (31), using previously reported ^{35}S-labeled riboprobes against *Runx2*, *Col1α1* (collagen 1α1), and *Bglap2* (osteocalcin) (9). To detect the expression of *Runx3*, we used an 846-bp probe that spanned the 3′ end of *Runx3* (nucleotides 1201 to 2047 of the sequence reported under NCBI RefSeq accession number NM_019732). Hybridization was performed at 55°C (overnight), and sections were washed at 63°C. Autoradiography and Hoechst 33258 staining were performed as previously described (52).

Bone histomorphometry. Static and dynamic histomorphometry was performed on tibiae and vertebrae of 3-month-old littermate mice. Three *Runx3* KO and WT mice were used for the static analyses, and four mice of both groups were used for the dynamic analyses. For assessment of dynamic indices, mice were injected with a freshly prepared calcein solution (catalog number C0875; Sigma) (1 mg/40 g mouse, intraperitoneally [i.p.]) 6 and 2 days before sacrifice. Data were collected with the OsteoMeasure and Trabecular Analysis systems (Osteometrics, Atlanta, GA). Data are reported in accordance with standard nomenclature (53).

Proliferation and apoptosis assays. To measure the OBL proliferation capacity, we used a bromodeoxyuridine (BrdU) incorporation assay on calvaria sections of 9-day-old *Runx3* KO and WT littermate mice, as previously described (54). Briefly, calvariae were fixed (4% paraformaldehyde [PFA] for 24 h) 12 h after BrdU injection (Sigma) (50 μg/g mouse). Following decalcification (14% EDTA for 48 h) and sucrose immersion (20% for 24 h), calvariae were embedded in an optimal-cutting-temperature (OCT) compound (Tissue-Tek), and 5-μm-thick coronal sections were made, fixed in PFA (4% for 20 min), treated with HCl (2 N for 30 min), and blocked (5% horse serum for 30 min). Sections were incubated with a rat anti-BrdU antibody (catalog number MCA2060; Serotec), followed by incubation with secondary Cy3-conjugated anti-mouse IgG (Jackson ImmunoResearch) and mounting (4′,6-diamidino-2-phenylindole [DAPI]-containing medium). Analysis was performed by counting BrdU-positive/DAPI-positive cells in ≥6 calvaria sections from each mouse.

To determine OBL apoptosis, we performed a transferase dUTP nick end labeling (TUNEL) assay on calvaria sections of 14-day-old *Runx3* KO and WT littermate mice, as described previously (54). Briefly, 5-μm-thick sections were prepared as described above for the BrdU procedure, and the TUNEL ApopTag kit (catalog number S7165; Millipore) was used according to the manufacturer's instructions. Counterstaining was performed with toluidine blue. Analysis was performed by counting TUNEL-positive cells in ≥5 calvaria sections from each mouse.

Culture and analysis of primary OBLs. Primary OBL cultures from bone marrow (BM) stromal cells (medullary cavities of humeri, femora, and tibiae) or calvariae were established from 2-month-old or 3- to 4-day-old mice (n = 4 or 5), respectively, as described previously (55, 56), and maintained for 21 to 28 days. *Runx3* expression in calvaria-derived OBL cultures was analyzed by Western blotting (see Fig. S1 in the supplemental material). For BM stromal cultures, immunodepletion of adherent CD11b$^+$ cells by fluorescence-activated cell sorter (FACS) sorting was performed (FACSAria sorter; BD) 14 days after initial plating (57). To induce osteogenesis, β-glycerophosphate (10 mM) and ascorbic acid (50 μg/ml) were added to culture medium 48 h after the start of culture. To assay bone mineralization, equal numbers of nucleated cells were plated, cultured, and stained with von Kossa stain (58) at different time points during culture growth. To quantify the relative mineralized area, digital images of whole plates were analyzed using ImagePro software (Media Cybernetics, MD). A CFU assay was performed on primary OBL cultures using an alkaline phosphatase (ALP) staining kit (catalog number 00-0009; Stemgent, CA), as described previously (59). ALP-positive colonies were counted in 10 random microscope fields (at a ×100 magnification) to determine osteoprogenitor cell numbers, as described previously(60).

Gene expression analyses. Total RNA was extracted from calvaria-derived primary OBL cultures of *Runx3*OBL and WT control mice using the RNeasy minikit (Qiagen, USA). The quality and quantity of RNA were determined using the Agilent 2100 bioanalyzer. RNA was then reverse transcribed, amplified, and labeled with an Affymetrix GeneChip whole-transcript sense target labeling kit. Gene expression data (GeneChip Mouse Gene 2.0 ST array system) were generated according to the manufacturer's protocols (Affymetrix, Santa Clara, CA). Hybridized arrays

were scanned using the Affymetrix GeneChip 3000 7G scanner. Custom software (GeneChip analysis suite) was used to analyze the intensity data and calculate a set of absolute metrics. Microarray data were normalized by the Partek genomic suite software. Data in CEL files, containing raw expression measurements, were preprocessed and normalized using the robust multichip average (RMA) algorithm (61). Over- and underexpression were defined as significant changes of ≥1.5-fold with a false discovery rate (FDR) q value of <0.1, applying analysis of variance (ANOVA). Selective validation of microarray expression results was conducted by reverse transcription-quantitative PCR (RT-qPCR), using the primers listed in Table S2 in the supplemental material.

RT-qPCR analysis. cDNA was synthesized with the QuantiTect reverse transcription kit (Qiagen, USA), using 1 μg of purified RNA, and analyzed by SYBR green qPCR using the miScript SYBR green PCR kit (Qiagen, USA) and the LightCycler 480 system (Roche, USA). Each RT-qPCR experiment consisted of >3 biological repeats using two independently prepared cDNA samples.

Statistical analysis. Data are presented as means and standard deviations (SD). Statistical analyses were performed with two-tailed Student's t test. Values were considered statistically significant at a P value of <0.05.

Microarray data accession number. Data sets were submitted to the Gene Expression Omnibus database (www.ncbi.nlm.nih.gov/geo) under accession number GSE57195.

RESULTS

Runx3-null mice show delayed skeletal ossification. To determine if Runx3 has a role in embryonic bone formation, we stained Runx3-null (*Runx3* KO) and wild-type (WT) littermate E18.5 skeletons with alizarin red S and alcian blue (50). Besides having apparently smaller skeletons, *Runx3* KO embryos showed delayed ossification of the hind- and forelimb distal bones (Fig. 1A, left) as well as of the mandible (angular process) and skull (Fig. 1A, right). Moreover, the intramembranous skull bones and clavicles of *Runx3* KO mice displayed significantly fainter alizarin red A (bone) staining and were apparently softer than those of WT littermate mice (see Fig. S2A in the supplemental material). These findings were also evident by comparative X-ray imaging of 23-day-old (D23) calvariae, demonstrating significant diminution of bone tissue in *Runx3* KO skulls (see Fig. S2B in the supplemental material). Comparative analyses of skeletons at earlier embryonic time points demonstrated that *Runx3* KO delayed bone ossification could be detected in the limb bone extremities and mandible as of E16.5 using alizarin red S and alcian blue staining (see Fig. S2C in the supplemental material). Notably, while still small, the skeletons of D7 *Runx3* KO mice displayed a WT-like ossification pattern (Fig. 1B), as previously reported (33). To further elucidate the role of Runx3 in skeletal development, we analyzed ossification kinetics in E18.5 and newborn (D0.5) heterozygote $Runx2^{+/-}$ mice with various *Runx3* gene dosages (+/+, +/−, or −/− genotype). Interestingly, although E18.5 $Runx2^{+/-}$ $Runx3^{-/-}$ embryos were generated at the expected Mendelian ratio, these mice showed considerable mortality, with only a few mice surviving to 1 week of age. Analysis revealed a gene dose dependence between *Runx3* and the extent of distal limb bone ossification (Fig. 1C). Specifically, while $Runx2^{+/-}$ mice showed progressive ossification of the palmar and plantar bones, digital bones of D0.5 $Runx2^{+/-}$ $Runx3^{-/-}$ mice remained grossly cartilaginous, with $Runx2^{+/-}$ $Runx3^{+/-}$ bones displaying an intermediate phenotype (Fig. 1C). Complementary analyses of E14.5 and E16.5 $Runx3^{+/-}$ $Runx2^{+/-}$ and $Runx3^{+/+}$ $Runx2^{+/-}$ developing skeletons (see Fig. S2D in the supplemental material) did not reveal differences in ossification patterns between these two genotypes. Taken together, these findings suggest that Runx3 might serve a nonredundant function in the ossification of the distal limb bones.

***Runx3* KO mice exhibit severe congenital osteopenia.** To complement the results of the perinatal analysis described above, we examined whole skeletons of adult *Runx3* KO and WT littermate mice using alizarin-alcian staining. Apart from their lasting smaller size, *Runx3* KO skeletons could not be distinguished from those of WT littermate mice (see Fig. S2E in the supplemental material). However, the apparent kyphosis, a skeletal condition clinically correlated with osteopenic bones (62) and prominent dwarfism of adult *Runx3* KO mice (Fig. 1D), as well as the above-mentioned perinatal intramembranous ossification deficits implied a possible osteoblastic involvement in this phenotype and prompted us to further analyze their bone characteristics.

We then analyzed bone structure and architecture by microcomputed tomography (μCT) imaging of femora from female *Runx3* KO and littermate WT mice (Fig. 1E and F). Because *Runx3* KO mice manifest colitis at 4 weeks of age (27), we examined bone cortical and trabecular indices of 3-week-old (precolitic) mice, to avoid colitis-associated effects (56, 63). Comparative μCT imaging revealed that long bones of *Runx3* KO mice were short and displayed significantly reduced cortical thickness and underdeveloped trabecular regions compared to those of WT mice (Fig. 1E). Quantitative analysis indicated that *Runx3* KO mice had a 19% reduction in femoral length ($P < 0.001$) (Fig. 1Fa) and a pronounced reduction in femoral width, manifested by a 50% smaller bone cortex area than that of WT littermate mice ($P < 0.001$) (Fig. 1Fb). Consequently, compared to the WT, *Runx3* KO bones displayed 41% and 34% decreases in thickness and total section area, respectively ($P < 0.001$) (Fig. 1Fc and d). Moreover, cortices of *Runx3* KO mice displayed the hallmarks of osteopenia, including 14% and 58% reductions in bone mineral density (BMD) and bone mineral content (BMC), respectively, compared to the WT ($P < 0.001$) (Fig. 1Fe and f). This osteopenic bone phenotype was also apparent in the cancellous region of *Runx3* KO femur, evidenced by significant decreases in trabecular thickness as well as in trabecular BMD and BMC (22%, 28%, and 59%, respectively) compared to the WT ($P < 0.001$) (Fig. 1Fg to i). Similar bone deficits were found in femora from male *Runx3* KO mice or $Runx3^{fl/fl}$/*Pgk*-cre mice (see Fig. S3 in the supplemental material), substantiating the association between the observed osteopenic phenotype and the loss of Runx3.

To address whether the decreases in BMD and BMC affect *Runx3* KO bone biomechanical properties, we measured bone rigidity of *Runx3* KO and WT long bones (see Fig. S4 in the supplemental material). Applying the 3-point bending method (64) on whole tibiae, we found a 33% reduction in Young's modulus, a size-corrected measure of bone material rigidity, for *Runx3* KO bone (70.12 N/m^2) compared to that for WT littermate bone (104.63 N/m^2). Because BMD correlates linearly with Young's modulus (65), the increased mechanical fragility of *Runx3* KO long bones not only confirmed the osteopenic phenotype but also underscored its biomedical impact.

We then determined the temporal onset of the *Runx3* KO bone defect by μCT analysis. Humeri of 1-day-old *Runx3* KO mice were shorter by 15% and their cortical region had 11% and 38% lower BMD and BMC, respectively, than those of WT littermate mice (Fig. 2A). Qualitative imaging of E18.5 femora revealed a substantial difference in the structural organization of *Runx3* KO long

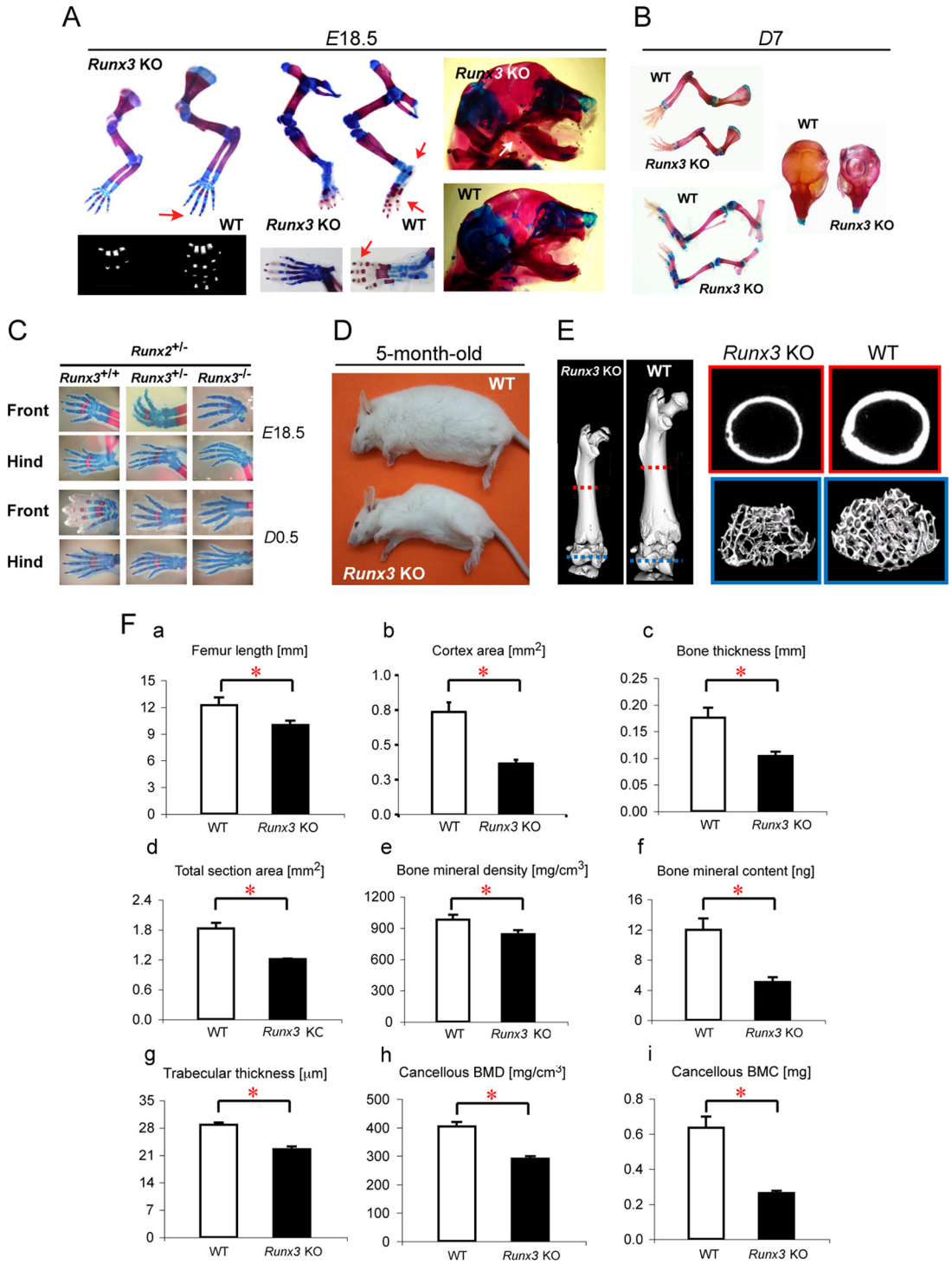

FIG 1 Phenotypic analysis of *Runx3* KO mouse bones. (A) Short stature and delayed ossification of the distal limb and mandibular bones of *Runx3* KO E18.5 embryos. Alizarin red S (bone) (purple)-alcian blue (cartilage) (blue) staining of forelimbs (left) and hindlimbs (middle) shows calcification of tarsal, metatarsal, and digital limb bones in a WT embryo (red arrows) and a lack of calcification in a *Runx3* KO embryo. Similar deficits are seen by comparative μCT imaging of the palmar bones (bottom left). Alizarin red S-alcian blue staining shows a complete lack of ossification of the angular process of the mandibular bone (right, white arrow) in an E18.5 *Runx3* KO embryo versus its apparent ossification in a WT littermate embryo. (B) The ossification pattern of a 7-day-old (D7) *Runx3* KO skeleton is indistinguishable from that of a WT skeleton. Alizarin red S-alcian blue staining shows a WT-like ossification pattern of the *Runx3* KO skeleton. Note the apparently smaller *Runx3* KO skeleton. (Top left) Front limbs; (bottom left) hind limbs; (right) skulls. (C) Gene dosage effect of *Runx3* on bone ossification in $Runx2^{+/-}$ mice. Shown is alizarin red S-alcian blue staining of E18.5 and D0.5 palm bones of $Runx2^{+/-}$ mice with either the $Runx3^{+/+}$, $Runx3^{+/-}$, or $Runx3^{-/-}$ genotype. Note the relationship between the *Runx3* dosage and the degree of ossification of the palmar and plantar bones at E18.5 and D0.5. (D) Short stature and kyphosis in adult *Runx3* KO mice. Pictures of 5-month-old *Runx3* KO and WT littermate mice show significantly smaller size and kyphosis in the *Runx3* KO mouse. (E) *Runx3* KO mice have short bones (left), thin cortices (top right), and underdeveloped trabecular cross sections (bottom right). Shown are representative 3D-reconstructed μCT images of femora of 23-day-old *Runx3* KO and WT mice. Dashed lines mark the cortical (red) and trabecular (blue) regions of interest (see Materials and Methods). (F) *Runx3* KO mice are severely osteopenic. Comparative μCT analyses of femora of 23-day-old *Runx3* KO and WT mice were performed. (a to f) Whole-bone and bone cortex parameters ($n = 6$ *Runx3* KO mice; $n = 11$ WT littermate mice); (g to i) cancellous bone parameters ($n = 4$ *Runx3* KO mice; $n = 6$ WT littermate mice). Values are means and SD. Asterisks indicate a P value of <0.01.

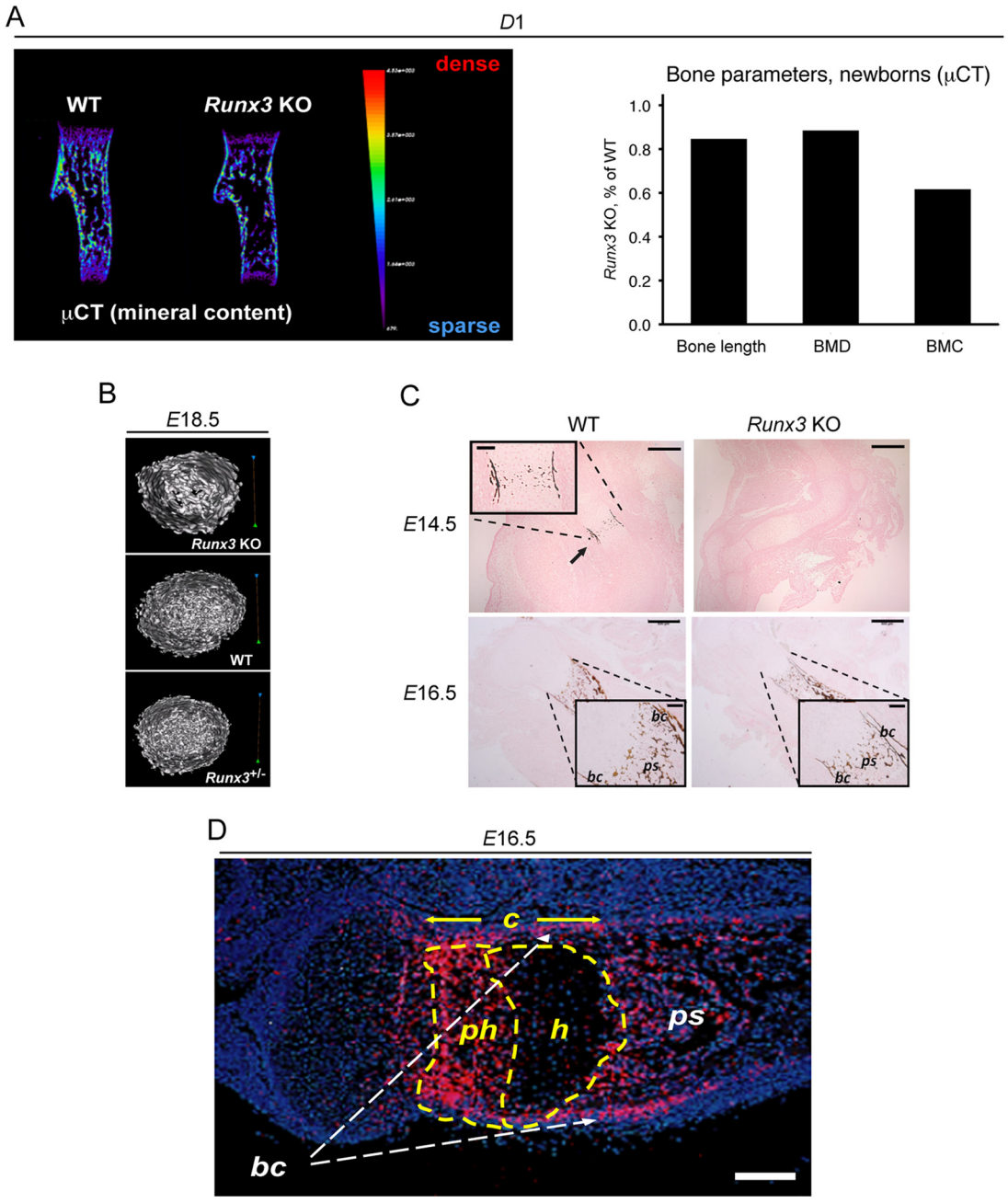

FIG 2 Temporal onset of *Runx3* KO osteopenia and *Runx3* expression in developing bone OBLs. (A) *Runx3* KO osteopenia is congenital. Comparative μCT analyses of humeri from D1 *Runx3* KO and WT littermate mice were performed. Images showing congenital osteopenia of both cortical and cancellous regions in humeri of *Runx3* KO versus WT mice (left) (the color bar indicates mineral content) and quantitative μCT structural analysis of these bones (right) are depicted. (B) Altered bone ultrastructure in E18.5 *Runx3* KO mice. Shown are μCT images of 50-μm-thick reconstructed midhumeral cross sections. *Runx3* KO mice (top) are compared to WT (middle) and *Runx3*$^{+/-}$ (bottom) littermate control mice. (C) Delayed ossification in E14.5 *Runx3* KO embryos. von Kossa-eosin staining of an E14.5 WT femoral section shows calcification in the bone collar (bc) and primary spongiosa (ps) regions (arrow), versus the complete lack of calcification in bone from an age-matched *Runx3* KO mouse (top row) (magnifications, ×40 for images and ×100 for inset). By E16.5, the ossification patterns in WT and *Runx3* KO femora were qualitatively indistinguishable (bottom row) (magnifications, ×40 for images and ×200 for insets). Bars, 500 μm (images), 125 μm (top inset), and 100 μm (bottom insets). (D) *Runx3* expression in developing bone OBLs. RNA *in situ* hybridization of an E16.5 humeral section demonstrates intense *Runx3* expression in primary spongiosa and bone collar OBLs. At this embryonic stage, *Runx3* expression is also detected in prehypertrophic (ph), but not in hypertrophic (h), chondrocytes (c) in the developing growth plate. *Runx3* signal intensity in OBLs is as high as that in prehypertrophic chondrocytes. Bar, 200 μm.

bones compared to that of long bones of WT and heterozygous littermates (Fig. 2B). Moreover, histological analysis of long bone mineralization at E14.5, the earliest time point of bone appearance, showed a complete lack of bone material in *Runx3* KO embryos, as opposed to bulk calcification in the WT embryo bone collar and primary spongiosa regions (Fig. 2C). However, staining of E16.5 *Runx3* KO bone sections showed mineral deposits in these regions (Fig. 2C), indicating that although delayed, osteo-

genesis in *Runx3* KO mice commenced by ~E16.5. Taken together, the delayed embryonic osteogenesis, the reduced cortical and cancellous BMD and BMC, and the decreased biomechanical strength demonstrate that *Runx3* KO mice are congenitally osteopenic. In summary, while *Runx3* KO femora appear outwardly normal, albeit significantly shorter than those of their WT counterparts, their cortical width axis and trabecular development are severely impaired. As these bone features are attained by OBL activity (5), these findings are consistent with the notion that loss of Runx3 is associated with osteoblastic dysfunction.

***Runx3* is expressed in developing bone OBLs.** We then determined *Runx3* expression in E16.5 embryonic long bones using ^{35}S-RISH. Osteoblastic *Runx3* expression was detected in OBLs of the developing bone collar and primary spongiosa regions (Fig. 2D), as was also found previously by Soung et al. (32). Significantly, the intensity of *Runx3* staining in OBLs was similar to that in prehypertrophic chondrocytes, an established *Runx3*-expressing cell population (24, 30), indicating a relatively high expression level of *Runx3* in developing bone OBLs.

Mice bearing OBL-specific *Runx3* inactivation recapitulate the osteopenic phenotype. To further evaluate Runx3 function in bone formation, we crossed *Runx3*$^{LoxP/LoxP}$ mice to transgenic *Col1*α*1*-cre mice, to generate mice that specifically lack Runx3 in OBLs (*Runx3*$^{fl/fl}$/*Col1*α*1*-cre; hereafter named *Runx3*OBL mice). *Runx3*OBL mice were born at the expected Mendelian ratio and had a 20 to 50% lower body mass than that of their WT littermates (Fig. 3A). Ossification deficits in *Runx3*OBL skeletons were similar to those found in *Runx3* KO mice, including the short stature that persisted throughout life (Fig. 3B). μCT analyses of femora from 23-day-old *Runx3*OBL mice showed a 21.7% lower bone thickness, a 25.0% smaller cortical area, and a 27.1% BMC than those of littermate control mice (Fig. 3C to E). Conversely, heterozygote *Runx3*$^{fl/+}$/*Col1*α*1*-cre mice had no overt skeletal abnormalities (see Fig. S5A in the supplemental material). Of note, similar morphological findings of severe congenital dwarfism and retarded growth were observed in *Runx3*$^{fl/fl}$/*Osx1*-cre mice (see Fig. S5B in the supplemental material), functional analogs of *Runx3*OBL mice. However, due to low survival rates of *Runx3*$^{fl/fl}$/*Osx1*-cre mice, we used the *Runx3*OBL line for our extensive bone analyses. Furthermore, the generation of 23-day-old *Runx3*OBL mice on a *Runx2*$^{+/-}$ background phenocopied the observed dwarfism of *Runx3*OBL mice (see Fig. S5C in the supplemental material), underscoring the unique function of Runx3 in OBL-derived skeletal elongation.

To address the possible contribution of *Runx3*$^{-/-}$ cartilage cells to the observed osteopenic phenotype of *Runx3* KO mice, we generated mice bearing chondrocyte-specific *Runx3* inactivation, by crossing *Runx3*$^{LoxP/LoxP}$ mice to transgenic *Col1*α*2*-cre mice (*Runx3*$^{fl/fl}$/*Col1*α*2*-cre; hereafter named *Runx3*CHN mice). Of note, only 2/7 *Runx3*CHN mice had short stature, and when present, this phenotype was milder than that for *Runx3*OBL mice (Fig. 3F). Comparative bone staining (Fig. 3G) and μCT analyses (Fig. 3H to J) did not reveal significant differences in bone development or structural parameters between *Runx3*CHN mice and WT littermate controls.

***Runx3* KO mouse osteopenia results from an OBL proliferation defect manifested by fewer active OBLs.** To assess whether the observed osteopenia of *Runx3* KO mice was due to a dysfunction and/or a reduced number of OBL cells, we analyzed bone structural parameters by quantitative histomorphometry (53). *Runx3* KO mice exhibited a significantly lower bone mass, evident by a 38% decrease in bone volume/total volume (BV/TV), than that of the WT controls ($P < 0.01$) (Fig. 4A). This bone mass reduction resulted from a diminution in OBL numbers, manifested by 38% and 34% reductions in the surface OBL/bone surface (Ob.S/BS; percentage of bone surface occupied by OBLs) and in the number of OBLs/bone perimeter (N.Ob/B.Pm), respectively (both $P = 0.02$) (Fig. 4B and C). Notably, no significant changes in the analogous osteoclast (OCL) parameters surface OCL/bone surface (Oc.S/BS) and number of OCLs/bone perimeter (N.Oc/B.Pm) were found (see Fig. S5D in the supplemental material), underscoring the OBL cell-autonomous nature of the observed *Runx3* KO bone lesion.

Dynamic histomorphometric analyses of *Runx3* KO bones revealed a 19% decrease in the mineral apposition rate (MAR) (Fig. 4D) as well as profound reductions of the mineralizing surface/bone surface (MS/BS) and the bone formation rate (BFR) of 59% and 68%, respectively, compared to values for the WT controls ($P < 0.01$) (Fig. 4E and F). These results show that while the loss of Runx3 mildly affects individual OBL activity, as reflected by the MAR, the marked reduction in the number of active OBLs (MS/BS) is the underlying cause for the largely diminished BFR and the resulting osteopenic phenotype.

To discern whether reduced OBL proliferation and/or enhanced apoptosis could explain the reduced number of OBLs in *Runx3* KO bones, we conducted BrdU incorporation and TUNEL staining assays using calvarial sections from newborn mice. The loss of Runx3 severely decreased the proliferation capacity of calvarial OBL progenitors, as reflected by a >50% reduction in the number of BrdU-positive cells compared to the WT (Fig. 4G). On the other hand, WT and *Runx3* KO calvarial sections had comparable numbers of TUNEL-positive nuclei (Fig. 4H). These results indicate that an impaired proliferation of *Runx3* KO OBL progenitor cells and not enhanced apoptosis led to the lower number of active OBLs.

Cultured Runx3-deficient OBLs display impaired proliferation and bone matrix formation. To directly evaluate whether a lack of Runx3 affects OBL formation and differentiation, we analyzed primary cultures of BM stromal cells. *In situ* ALP staining revealed similar numbers of ALP-positive osteoprogenitor-derived colonies in 3-week-old *Runx3*OBL and WT cultures (Fig. 5A), suggesting that the commitment to the osteoblastic lineage is independent of Runx3. However, the size of the ALP-positive colonies in *Runx3*OBL cultures was 75% smaller than that in WT cultures (Fig. 5A), indicating that their OBL lineage cell generation capacity was impaired. These *in vitro* results support our above-described histomorphometric measurements indicating that the reduced osteogenic activity in *Runx3* KO mice was due to lower numbers of active OBLs.

We then assessed OBL function by recording the mineralization capacities of stromal cultures derived from *Runx3* KO, *Runx3*OBL, and WT mice. At 21 days, *Runx3* KO BM stromal cultures yielded a 52% smaller mineralized area than that of cultures derived from WT mice (Fig. 5B). Similarly, at 28 days, *Runx3*OBL BM stromal cultures showed a 59% decrease in the formation of mineralized nodules compared to WT cultures (Fig. 5C). Significantly, an even more striking reduction in bone matrix formation was noted when OBLs from calvariae of newborn *Runx3*OBL mice were cultured for 21 days (Fig. 5D), yielding almost no mineralized nodules, compared to cultures from new-

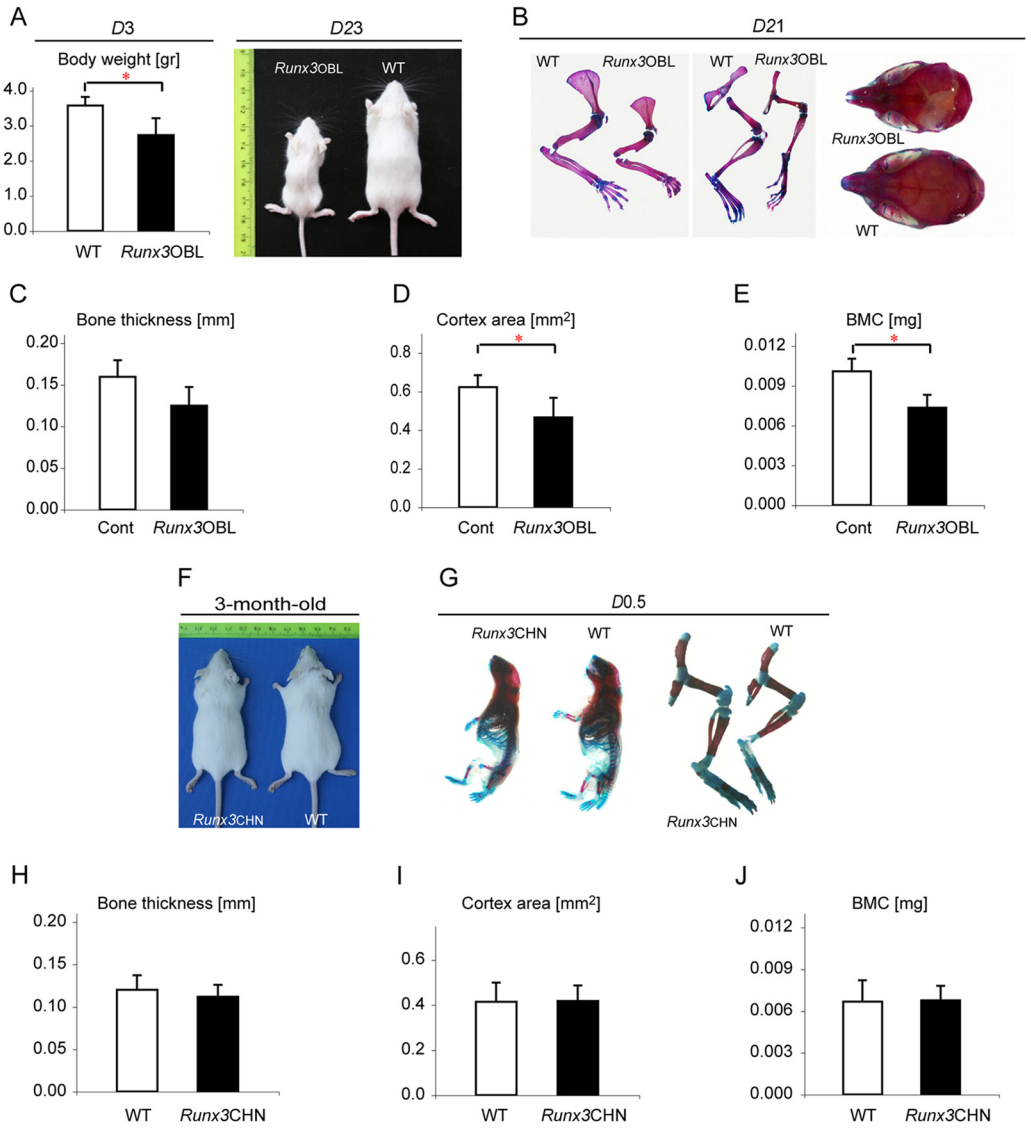

FIG 3 The *Runx3* KO osteopenic phenotype is recapitulated in *Runx3*OBL but not in *Runx3*CHN mice. (A) *Runx3*OBL mice recapitulate the *Runx3* KO skeletal phenotype. The decreased body weight and short stature of *Runx3*OBL mice are indicated. Body weights of D3 mice (left) ($n = 6$ mice/genotype) and representative gross appearances at D23 (right) are shown. (B) Alizarin red S-alcian blue staining of D21 *Runx3*OBL and WT mice showing similar ossification patterns with distinct size differences. (Left) Front limb; (middle) hind limb; (right) skull. (C to E) *Runx3*OBL mice exhibit an osteopenic phenotype. μCT analysis of D23 *Runx3*OBL ($n = 2$) and control littermate (WT and $Runx3^{fl/+}$/*Col1a1*-cre) ($n = 5$) female mice was performed. (C) Bone thickness; (D) cortex area; (E) BMC. Values are means and SD. Asterisks indicate statistical significance ($P < 0.01$). (F) *Runx3*CHN mice are seemingly indistinguishable from WT littermate mice. Shown are 3-month-old mice. (G) Similar ossification patterns in *Runx3*CHN and WT mice. Shown are whole skeleton (left) and hind limbs (right) of alizarin red S-alcian blue-stained D0.5 mice. (H to J) Comparable bone parameters for *Runx3*CHN and WT littermate mice. μCT analysis of D23 *Runx3*CHN mice ($n = 2$) and WT littermate controls ($n = 5$) was performed. (H) Bone thickness; (I) cortex area; (J) BMC. Values are means and SD, and asterisks indicate statistical significance ($P < 0.01$).

born WT mice. Collectively, these *in vitro* experiments demonstrate that the proliferation capacity of Runx3-deficient OBL progenitors is impaired, leading to a substantial decrease in the number of active OBLs, which results in reduced bone matrix formation.

Expression of major OBL markers and transcriptome analysis. Using RISH, we determined the *in vivo* expression levels of selected OBL markers in femoral sections of 3-day-old *Runx3* KO and WT mice. Compared to WT mice, a substantial decrease in expression levels was noted in bone regions where mRNAs of the early OBL markers *Col1α1* and *Runx2* and the mature OBL marker *Bglap2* (osteocalcin gene) were expressed (37, 62) (Fig. 6A). These reduced expression levels in OBL-occupied areas correspond to our above-described findings of diminished OBL numbers and consequent low bone-forming ability in *Runx3* KO mice.

We next sought to gain insight into the transcriptional program involved in precipitating the Runx3-deficient osteopenic phenotype. Consequently, we compared gene expression profiles in primary calvarial OBLs from *Runx3*OBL and littermate WT mice. Using a >1.5-fold change and an FDR q value of <0.1, relative to the control, as criteria for significance, we identified 351

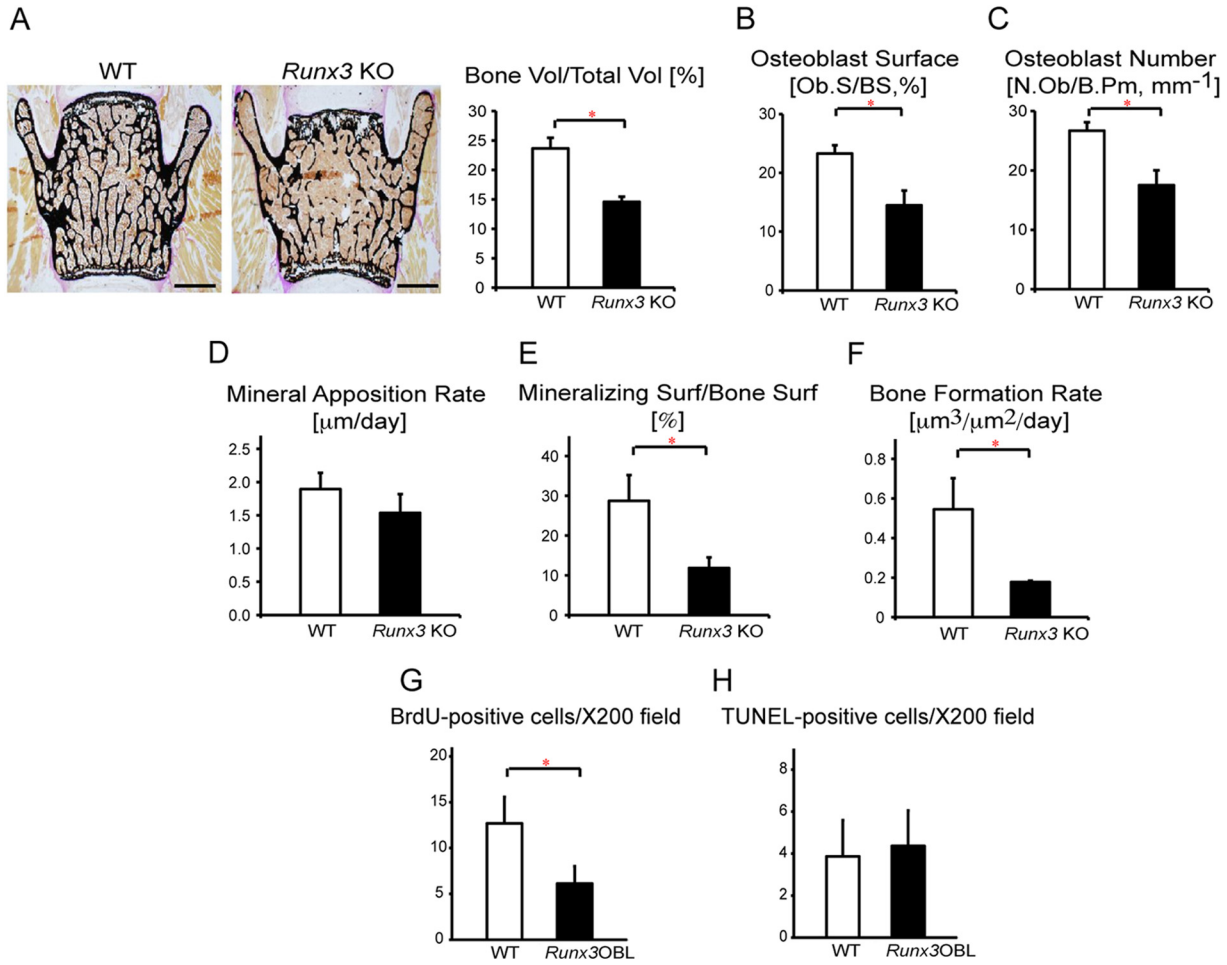

FIG 4 Comparative histomorphometry and OBL proliferation/apoptosis analyses. (A) Reduced bone volume in *Runx3* KO mice. Shown are images of von Kossa-stained vertebral sections of 3-month-old *Runx3* KO and WT littermate mice (left) (magnification, ×40; bar, 500 μm) and trabecular bone volume quantification (right) ($n = 3$ mice/genotype). Values are means and SD, and asterisks indicate statistical significance ($P < 0.01$). (B to F) Bone formation rates in 3-month-old *Runx3* KO and WT littermate mice indicating a significant reduction in the number of active OBLs and a diminished bone formation rate in *Runx3* KO mice. (B) Osteoblast surface (Ob.S). BS, bone surface. (C) Number of osteoblasts (N.Ob). B.Pm, bone perimeter. (D) Mineral apposition rate. (E) Mineralizing surface/bone surface. (F) Bone formation rate ($n = 3$ mice/genotype for panels B and C; $n = 4$ mice/genotype for panels D to F). Values are means and SD, and asterisks indicate statistical significance ($P < 0.01$). (G) Impaired OBL proliferation rate in *Runx3*OBL mice. Comparative BrdU incorporation assays using calvaria sections from 9-day-old *Runx3*OBL ($n = 1$) and WT ($n = 4$) littermate mice show significant reductions in proliferating OBLs in *Runx3*OBL mice. BrdU incorporation was determined for ≥6 calvaria sections/mouse. Values are means and SD, and asterisks indicate statistical significance ($P < 0.01$). (H) Comparable OBL apoptosis rates in *Runx3*OBL and WT littermate mice. OBL apoptosis was determined by a TUNEL assay using calvaria sections from 14-day-old mice ($n = 2$ mice/genotype; ≥6 calvaria sections per mouse). Values are means and SD.

differentially expressed genes, of which 202 were upregulated and 149 were downregulated, in cultured OBLs from *Runx3*OBL mice (Fig. 6B; see also Table S1 in the supplemental material). Of note, a pronounced decrease in the levels of marker genes characteristic of active OBLs was noted (see Table S1 in the supplemental material). For example, there was a 5.2-fold reduction in the level of the matrix metallopeptidase 3 gene *Mmp3* (66, 67), a 3.2-fold reduction in the level of the tyrosine phosphatase receptor type Z polypeptide 1 gene *Ptprz1* (68), and a 3.1-fold reduction in the level of the dentin matrix protein 1 gene *Dmp1* (69). In addition, substantial increases in the levels of key components of the Notch signaling pathway were found, including 3.3- and 5.9-fold increases in the levels of the TF genes *Hes1* (Hairy enhancer of split 1) and *Hey1* (Hes-related with YRPW motif), respectively (Fig. 6B; see also Table S1 in the supplemental material). Of note, transgenic overexpression of *Hes1* results in osteopenia due to decreased OBL activity (70), while inhibition of canonical Notch signaling increased osteoblast numbers and BMD (71). The differential expression of several of these osteoblastogenesis signature markers was further validated by RT-qPCR (Fig. 6C). Together, the *in situ* hybridization results and gene expression data support the notion that the lack of Runx3 impairs OBL generation, leading to the observed osteopenic phenotype.

DISCUSSION

This study describes a novel function of *Runx3* in murine osteoblastogenesis. Using mouse genetic models, we show that loss of Runx3 in precommitted OBLs diminishes the formation of active/mature OBLs and consequently leads to severe congenital osteopenia and dwarfism. Bones of Runx3-deficient mice are sig-

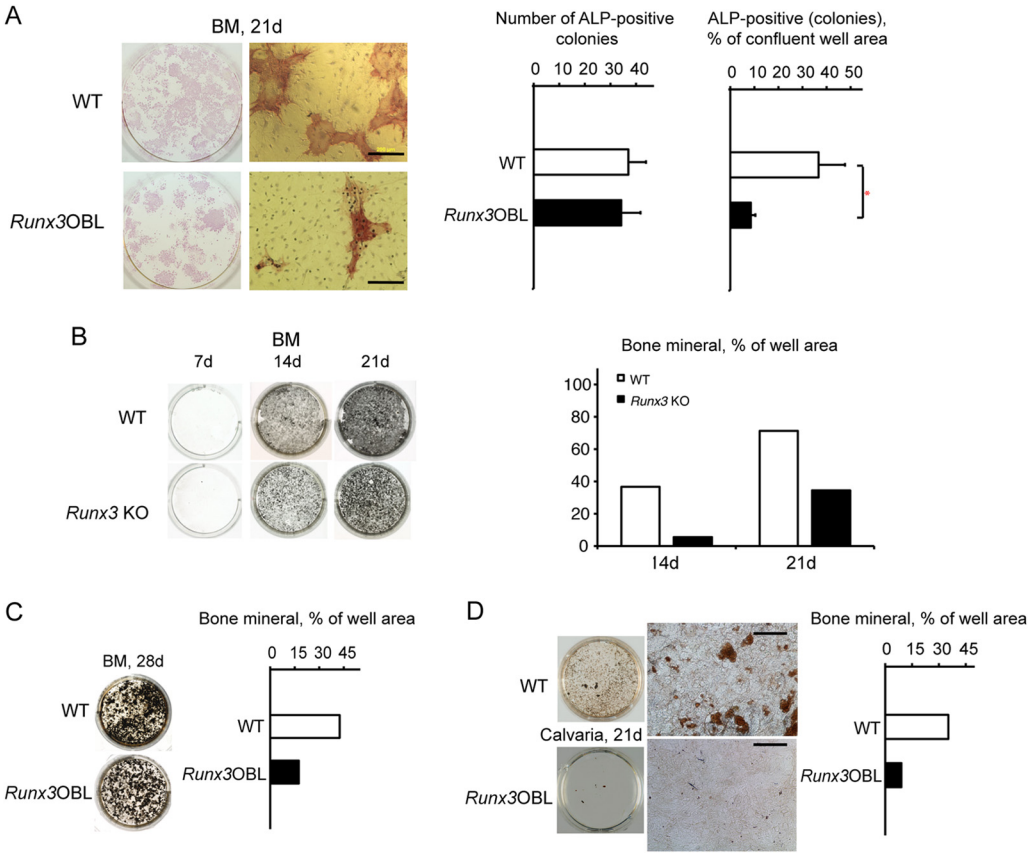

FIG 5 Growth rate and mineral deposition analysis of cultured Runx3-null OBLs. (A) Reduced number of active OBLs in *Runx3*OBL BM stromal cultures. Total BM cells were cultured to confluence for 21 days (21d) and stained with ALP. (Left) Whole-plate and magnified (×200) images. Bar, 200 μm. (Middle) Osteoprogenitor cell numbers were determined by counting ALP-positive colonies (>10 cells) in 10 microscope fields at a ×100 magnification. (Right) The number of OBL lineage cells generated from these osteoprogenitor colonies was deduced by determining the cumulative area of ALP-positive colonies per whole-plate area. Data shown represent data from three independent experiments with similar findings. Values are means and SD, and asterisks indicate statistical significance ($P < 0.01$). (B) Impaired mineralization capacity of cultured *Runx3* KO BM OBLs. Following plating, the mineral deposition capacity of *Runx3* KO and WT BM-derived OBL cultures was determined at 7-day intervals. Shown are whole-plate images (von Kossa staining) (left) and digital quantification of mineralized nodules (black) at 14 and 21 days of culture (right). Data shown represent data from two independent experiments with similar findings. (C) Cultured BM OBLs from *Runx3*OBL mice display a markedly reduced mineral deposition capacity. Shown are whole-plate images of 28-day cultures (von Kossa staining) (left) and digital enumeration (right). Data shown represent data from two independent experiments with similar findings. (D) Calvaria-derived OBL cultures exhibit a diminished mineralization capacity. Mineral staining (von Kossa) of 21-day-old confluent OBL cultures isolated from calvariae of WT and *Runx3*OBL mice was performed. Shown are images of whole plates (left), a microscopic view of an enlarged plate area (middle) (magnification, ×100; bar, 400 μm), and whole-plate digital quantification of mineral deposition (right). Data shown represent data from two independent experiments with similar findings. Values are means and SD. Note that both *Runx3*OBL and WT culture images were taken under the same settings. The difference in clarity is due to the fact that in the WT culture plate, the brown mineralized (~35% of the plate) nodules cast shadows that enhanced the contrast of neighboring cells. This effect does not exist in the KO plate, where mineralization was significantly reduced (~9% of the plate).

nificantly underdeveloped, and their strength is profoundly compromised. Although the majority of cases of human congenital dwarfism are related to defects in growth plate chondrocytes (72), the skeletal phenotype presented here highlights a somewhat overlooked OBL function in normal bone elongation (73, 74).

The human *RUNX3* gene resides on chromosome 1p36, a locus that is associated with low BMD and osteoporosis in humans. Initially recognized by a whole-genome linkage scan analysis (39), this genomic region was independently confirmed to contain a quantitative trait locus for bone-related defects by numerous other studies (40–45). Moreover, similar findings on the linkage of mouse chromosome 4q, syntenic to the human 1p region, to low BMD were also reported previously (75, 76). Ongoing screenings for susceptibility genes that reside at the 1p36 locus identified several candidates, including *TNFRSF1B* (77), *NPPB* (78), *MTHFR* (79), *WNT4*, and *ZBTB40* (45), suggesting that multiple genes, individually or in combination, contribute to the 1p36-associated low-BMD phenotype (80). It is therefore tempting to speculate, based on the findings described in this study, that RUNX3 deficiency might also affect human bone mineralization and thus may constitute a risk factor for low BMD/osteopenia in humans.

Previous studies have shown delayed chondrocyte differentiation/maturation and vascular invasion in E15.5 *Runx3* KO bones (32, 33). Probing the later phases of skeletogenesis, we observed transient mineralization delays for the distal limb bones and mandible in E16.5 *Runx3* KO embryos as well as for the intramembranous skull bones and clavicles in E18.5 *Runx3* KO embryos. The finding that this mineralization deficit recovered in postnatal *Runx3* KO mice could be explained by Runx2/Runx3 redundancy

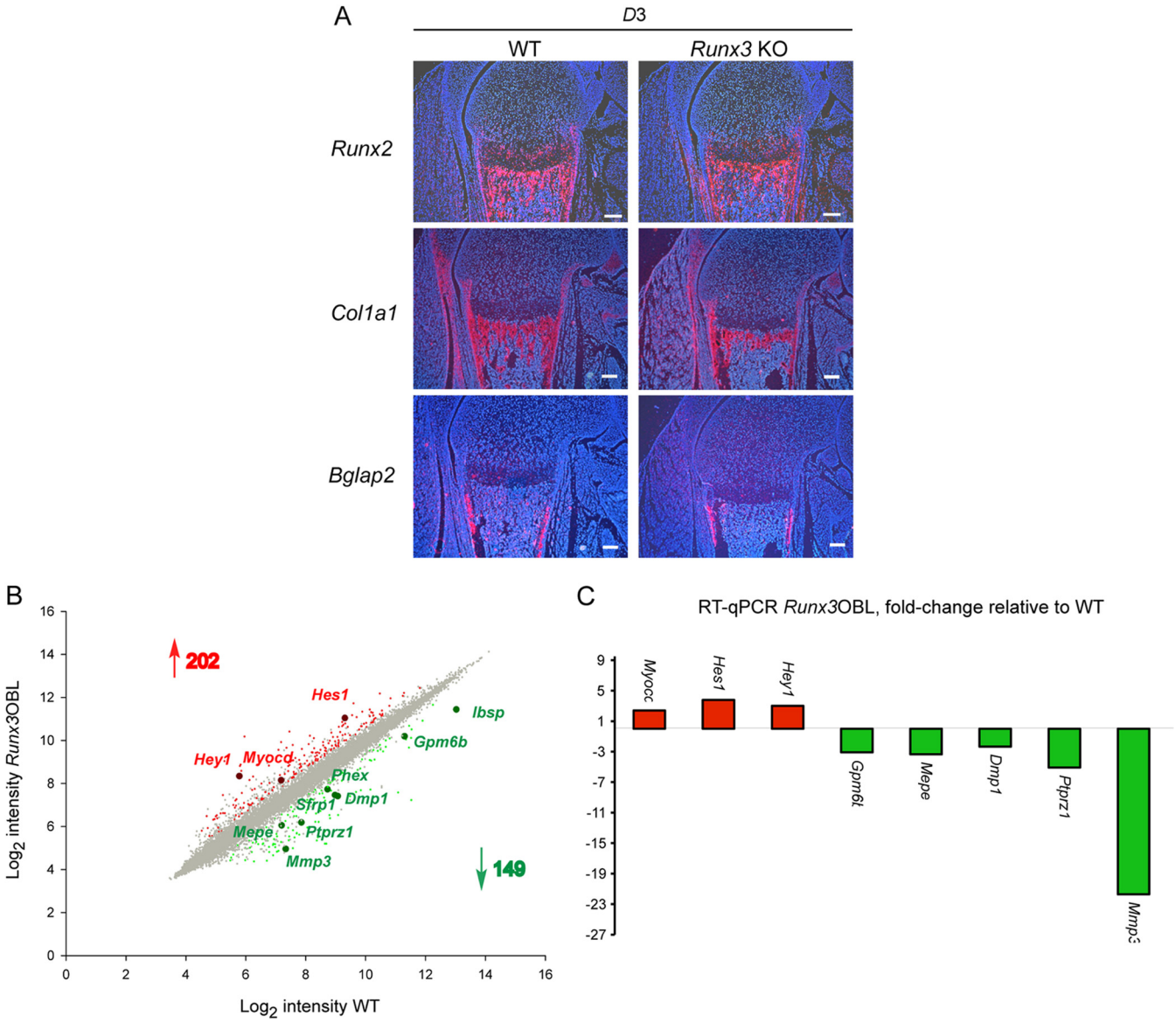

FIG 6 OBL markers and gene expression analysis. (A) Comparative expression analysis of OBL markers. Femoral sections from D3 *Runx3* KO and WT mice were used for ^{35}S-RISH (magnification, ×40; bar, 100 μm). Decreased bone areas where marker genes are expressed in *Runx3* KO bone sections reflect the lower numbers of OBLs in these mice. (B) Scatter plot of differentially expressed genes in calvaria-derived OBLs from *Runx3*OBL versus WT mice. Shown are gene expression levels ($\log_2$ scale) in *Runx3*OBL versus WT OBLs. Significantly increased and decreased expression levels of genes are indicated in red and green, respectively. Enlarged circles indicate Runx3-responsive genes that are known to participate in osteoblastogenesis. (C) Validation of several differentially expressed OBL genes. RT-qPCR analyses of RNA isolated from WT and *Runx3*OBL calvaria cultures showed gene expression trends similar to those observed by gene expression chip analysis.

in this process. This possibility is supported by the observation that the decline in palm bone ossification is associated with *Runx2*/*Runx3* gene dosage. Furthermore, the specific ablation of *Runx3* in chondrocytes (*Runx3*CHN mice), the main drivers of longitudinal bone growth (34), did not produce a notable defect in bone development or structure. This finding could be explained by the dominance of Runx2 in chondrocyte maturation (33), a notion that corresponds with perinatal lethality in chondrocyte-specific Runx2-deficient mice (14, 15).

Our preliminary observations of delayed ossification in the distal limb bones, clavicles, mandibles, and skull of *Runx3* KO and compound *Runx3*/*Runx2* developing skeletons were made using qualitative bone staining. Subsequently, these findings were supported by quantitative μCT and biomechanical analyses of long bones, revealing their severe congenital osteopenia. Although these data suggest that Runx3 is involved in the ossification of both endochondral and intramembranous bones throughout the developing skeleton, our initial finding of delayed palmar/plantar bone ossification in *Runx3* KO embryos might point to a more prominent function of Runx3 in the bones of the limb extremities. Interestingly, *Runx3* and *Runx2* were previously shown to be co-expressed in the developing digits of E14.5 mice, and *Runx3* was reported to be intensely expressed in the digits of E14.5 *Runx2*$^{-/-}$ mice, implying its Runx2-independent regulation at this site (81).

Thus, as opposed to the bone-defining functions of Runx2 (10), whose partial or complete deletion results in cleidocranial dysplasia or complete lack of bone, respectively, the absence of Runx3 seems to cause a less dramatic and yet persistent skeletal phenotype.

By employing immunohistochemistry on limb sections from E15.5 to E16.5 mice, Soung et al. reported the expression of *Runx3* in bone collar and primary spongiosa OBLs (32), in agreement with our RISH findings. Several other reports describe osteoblastic *Runx3* expression in murine embryonic perichondrium (81) and OBL lineage cells (3), as well as in human OBLs (82). However, to the best of our knowledge, this study is the first to assign a distinct function to Runx3 in these bone-forming cells.

OBL abundance is determined by several factors: the proliferation rate of OBL precursors, their capacity to differentiate toward mature OBLs, and the death rate of mature cells (3). Thus, elements that govern these events determine the active OBL pool size and play a major role in new bone formation. Three independent lines of evidence support the finding that osteoblastic loss of Runx3 significantly reduces the numbers of active OBLs: (i) the marked reduction in MS/BS, determined by *ex vivo* histomorphometry (with a mildly changed MAR); (ii) the diminished mineralization in long bone- and calvaria-derived cultured OBL progenitors; and (iii) the profound reductions in the levels of OBL maturation marker genes in transcriptome analyses of cultured OBLs. This diminished production of active OBLs stems from a proliferation defect, as evidenced by the reduced BrdU incorporation, rather than from a smaller mesenchymal progenitor pool size in the BM of Runx3-deficient mice. Furthermore, comparative examination of *Runx3*OBL culture phenotypes implied that while calvaria OBLs were profoundly dependent on Runx3 for their mineralizing function, its requirement by OBLs derived from long bone stromal progenitors was much less stringent. Notably, a similar spatial requirement was reported previously for Runx2 (11). In this case, haploinsufficiency severely affected intramembranous bones, leading to cleidocranial dysplasia in humans and mice, but mildly impacted endochondral bones.

In summary, our findings show that an OBL cell-autonomous function of Runx3 is required for mouse osteoblastogenesis. Runx3 function is required, along with and independent of Runx2, similar to their requirements in chondrogenesis. Thus, it appears that while Runx2 is mandatory for progenitor cell commitment to the osteoblastic lineage (14), Runx3 is nonredundantly required for the proliferation of these precommitted cells, to generate adequate numbers of active OBLs. Hence, in the absence of Runx3, OBL numbers are significantly reduced, while their individual cell function is only marginally affected. This low number of active OBLs impairs proper bone formation and causes severe congenital osteopenia and lifelong short stature in Runx3-deficient mice. Thus, whether RUNX3 deficiency also constitutes a risk factor for low BMD in humans remains to be addressed.

ACKNOWLEDGMENTS

This study was supported by a grant from the Israel Science Foundation (ISF) to Y.G.

We thank Tamara Berkuzki and Calanit Ra'anan for their valuable technical assistance; Ron Rotkopf and Kfir Umansky for help in computational analyses; Avraham Keter, Arie Gumberof, and Ofir Higfa for help in animal husbandry; and Eli Zelzer for the *Runx2*$^{+/-}$, *Col1α1*-cre, *Col1α2*-cre, and *Osx1*-cre mouse lines and his helpful suggestions and stimulating discussions throughout this work.

REFERENCES

1. **Karsenty G, Kronenberg HM, Settembre C.** 2009. Genetic control of bone formation. Annu Rev Cell Dev Biol **25:**629–648. http://dx.doi.org/10.1146/annurev.cellbio.042308.113308.
2. **Marie PJ.** 2008. Transcription factors controlling osteoblastogenesis. Arch Biochem Biophys **473:**98–105. http://dx.doi.org/10.1016/j.abb.2008.02.030.
3. **Lian JB, Javed A, Zaidi SK, Lengner C, Montecino M, van Wijnen AJ, Stein JL, Stein GS.** 2004. Regulatory controls for osteoblast growth and differentiation: role of Runx/Cbfa/AML factors. Crit Rev Eukaryot Gene Expr **14:**1–41. http://dx.doi.org/10.1615/CritRevEukaryotGeneExpr.v14.i12.10.
4. **Maes C, Kobayashi T, Selig MK, Torrekens S, Roth SI, Mackem S, Carmeliet G, Kronenberg HM.** 2010. Osteoblast precursors, but not mature osteoblasts, move into developing and fractured bones along with invading blood vessels. Dev Cell **19:**329–344. http://dx.doi.org/10.1016/j.devcel.2010.07.010.
5. **Rauch F.** 2005. Bone growth in length and width: the yin and yang of bone stability. J Musculoskelet Neuronal Interact **5:**194–201.
6. **Karsenty G.** 2008. Transcriptional control of skeletogenesis. Annu Rev Genomics Hum Genet **9:**183–196. http://dx.doi.org/10.1146/annurev.genom.9.081307.164437.
7. **Huang W, Yang S, Shao J, Li YP.** 2007. Signaling and transcriptional regulation in osteoblast commitment and differentiation. Front Biosci **12:**3068–3092. http://dx.doi.org/10.2741/2296.
8. **Long F.** 2012. Building strong bones: molecular regulation of the osteoblast lineage. Nat Rev Mol Cell Biol **13:**27–38. http://dx.doi.org/10.1038/nrm3254.
9. **Ducy P, Zhang R, Geoffroy V, Ridall AL, Karsenty G.** 1997. Osf2/Cbfa1: a transcriptional activator of osteoblast differentiation. Cell **89:**747–754. http://dx.doi.org/10.1016/S0092-8674(00)80257-3.
10. **Komori T, Yagi H, Nomura S, Yamaguchi A, Sasaki K, Deguchi K, Shimizu Y, Bronson RT, Gao YH, Inada M, Sato M, Okamoto R, Kitamura Y, Yoshiki S, Kishimoto T.** 1997. Targeted disruption of Cbfa1 results in a complete lack of bone formation owing to maturational arrest of osteoblasts. Cell **89:**755–764. http://dx.doi.org/10.1016/S0092-8674(00)80258-5.
11. **Otto F, Thornell AP, Crompton T, Denzel A, Gilmour KC, Rosewell IR, Stamp GW, Beddington RS, Mundlos S, Olsen BR, Selby PB, Owen MJ.** 1997. Cbfa1, a candidate gene for cleidocranial dysplasia syndrome, is essential for osteoblast differentiation and bone development. Cell **89:**765–771. http://dx.doi.org/10.1016/S0092-8674(00)80259-7.
12. **Liu W, Toyosawa S, Furuichi T, Kanatani N, Yoshida C, Liu Y, Himeno M, Narai S, Yamaguchi A, Komori T.** 2001. Overexpression of Cbfa1 in osteoblasts inhibits osteoblast maturation and causes osteopenia with multiple fractures. J Cell Biol **155:**157–166. http://dx.doi.org/10.1083/jcb.200105052.
13. **Kanatani N, Fujita T, Fukuyama R, Liu W, Yoshida CA, Moriishi T, Yamana K, Miyazaki T, Toyosawa S, Komori T.** 2006. Cbf-beta regulates Runx2 function isoform-dependently in postnatal bone development. Dev Biol **296:**48–61. http://dx.doi.org/10.1016/j.ydbio.2006.03.039.
14. **Takarada T, Hinoi E, Nakazato R, Ochi H, Xu C, Tsuchikane A, Takeda S, Karsenty G, Abe T, Kiyonari H, Yoneda Y.** 2013. An analysis of skeletal development in osteoblast-specific and chondrocyte-specific runt-related transcription factor-2 (Runx2) knockout mice. J Bone Miner Res **28:**2064–2069. http://dx.doi.org/10.1002/jbmr.1945.
15. **Adhami MD, Rashid H, Chen H, Clarke JC, Yang Y, Javed A.** 2015. Loss of Runx2 in committed osteoblasts impairs postnatal skeletogenesis. J Bone Miner Res **30:**71–82. http://dx.doi.org/10.1002/jbmr.2321.
16. **Levanon D, Groner Y.** 2004. Structure and regulated expression of mammalian RUNX genes. Oncogene **23:**4211–4219. http://dx.doi.org/10.1038/sj.onc.1207670.
17. **de Bruijn MF, Speck NA.** 2004. Core-binding factors in hematopoiesis and immune function. Oncogene **23:**4238–4248. http://dx.doi.org/10.1038/sj.onc.1207763.
18. **Chen W, Ma J, Zhu G, Jules J, Wu M, McConnell M, Tian F, Paulson C, Zhou X, Wang L, Li YR.** 2014. Cbfbeta deletion in mice recapitulates cleidocranial dysplasia and reveals multiple functions of Cbfbeta required

for skeletal development. Proc Natl Acad Sci U S A **111:**8482–8487. http://dx.doi.org/10.1073/pnas.1310617111.

19. **Qin X, Jiang Q, Matsuo Y, Kawane T, Komori H, Moriishi T, Tanaiuchi I, Ito K, Kawai Y, Rokutanda S, Izumi S, Komoti T.** 29 September 2014. Cbfb regulates bone development by stabilizing Runx family proteins. J Bone Miner Res http://dx.doi.org/10.1002/jbmr.2379.
20. **Lim KE, Park NR, Che X, Han MS, Jeong JH, Kim SY, Park CY, Akiyama H, Kim JE, Ryoo HM, Stein JL, Lian JB, Stein GS, Choi JY.** 31 October 2014. Core binding factor β of osteoblasts maintains cortical bone mass via stabilization of Runx2 in mice. J Bone Miner Res http://dx.doi.org/10.1002/jbmr.2397.
21. **Bangsow C, Rubins N, Glusman G, Bernstein Y, Negreanu V, Goldenberg D, Lotem J, Ben-Asher E, Lancet D, Levanon D, Groner Y.** 2001. The RUNX3 gene—sequence, structure and regulated expression. Gene **279:**221–232. http://dx.doi.org/10.1016/S0378-1119(01)00760-0.
22. **Levanon D, Glusman G, Bettoun D, Ben-Asher E, Negreanu V, Bernstein Y, Harris-Cerruti C, Brenner O, Eilam R, Lotem J, Fainaru O, Goldenberg D, Pozner A, Woolf E, Xiao C, Yarmus M, Groner Y.** 2003. Phylogenesis and regulated expression of the RUNT domain transcription factors RUNX1 and RUNX3. Blood Cells Mol Dis **30:**161–163. http://dx.doi.org/10.1016/S1079-9796(03)00023-8.
23. **Sullivan JC, Sher D, Eisenstein M, Shigesada K, Reitzel AM, Marlow H, Levanon D, Groner Y, Finnerty JR, Gat U.** 2008. The evolutionary origin of the Runx/CBFbeta transcription factors—studies of the most basal metazoans. BMC Evol Biol **8:**228. http://dx.doi.org/10.1186/1471-2148-8-228.
24. **Levanon D, Brenner O, Negreanu V, Bettoun D, Woolf E, Eilam R, Lotem J, Gat U, Otto F, Speck N, Groner Y.** 2001. Spatial and temporal expression pattern of Runx3 (Aml2) and Runx1 (Aml1) indicates non-redundant functions during mouse embryogenesis. Mech Dev **109:**413–417. http://dx.doi.org/10.1016/S0925-4773(01)00537-8.
25. **Yamashiro T, Aberg T, Levanon D, Groner Y, Thesleff I.** 2002. Expression of Runx1, -2 and -3 during tooth, palate and craniofacial bone development. Mech Dev **119**(Suppl 1)**:**S107–S110. http://dx.doi.org/10.1016/S0925-4773(03)00101-1.
26. **Levanon D, Bettoun D, Harris-Cerruti C, Woolf E, Negreanu V, Eilam R, Bernstein Y, Goldenberg D, Xiao C, Fliegauf M, Kremer E, Otto F, Brenner O, Lev-Tov A, Groner Y.** 2002. The Runx3 transcription factor regulates development and survival of TrkC dorsal root ganglia neurons. EMBO J **21:**3454–3463. http://dx.doi.org/10.1093/emboj/cdf370.
27. **Brenner O, Levanon D, Negreanu V, Golubkov O, Fainaru O, Woolf E, Groner Y.** 2004. Loss of Runx3 function in leukocytes is associated with spontaneously developed colitis and gastric mucosal hyperplasia. Proc Natl Acad Sci U S A **101:**16016–16021. http://dx.doi.org/10.1073/pnas.0407180101.
28. **Fainaru O, Woolf E, Lotem J, Yarmus M, Brenner O, Goldenberg D, Negreanu V, Bernstein Y, Levanon D, Jung S, Groner Y.** 2004. Runx3 regulates mouse TGF-beta-mediated dendritic cell function and its absence results in airway inflammation. EMBO J **23:**969–979. http://dx.doi.org/10.1038/sj.emboj.7600085.
29. **Fainaru O, Shseyov D, Hantisteanu S, Groner Y.** 2005. Accelerated chemokine receptor 7-mediated dendritic cell migration in Runx3 knockout mice and the spontaneous development of asthma-like disease. Proc Natl Acad Sci U S A **102:**10598–10603. http://dx.doi.org/10.1073/pnas.0504787102.
30. **Yoshida CA, Komori T.** 2005. Role of Runx proteins in chondrogenesis. Crit Rev Eukaryot Gene Expr **15:**243–254. http://dx.doi.org/10.1615/CritRevEukarGeneExpr.v15.i3.60.
31. **Sato S, Kimura A, Ozdemir J, Asou Y, Miyazaki M, Jinno T, Ae K, Liu X, Osaki M, Takeuchi Y, Fukumoto S, Kawaguchi H, Haro H, Shinomiya KI, Karsenty G, Takeda S.** 2008. The distinct role of the Runx proteins in chondrocyte differentiation and intervertebral disc degeneration: findings in murine models and in human disease. Arthritis Rheum **58:**2764–2775. http://dx.doi.org/10.1002/art.23805.
32. **Soung DY, Dong Y, Wang Y, Zuscik MJ, Schwarz EM, O'Keefe RJ, Drissi H.** 2007. Runx3/AML2/Cbfa3 regulates early and late chondrocyte differentiation. J Bone Miner Res **22:**1260–1270. http://dx.doi.org/10.1359/jbmr.070502.
33. **Yoshida CA, Yamamoto H, Fujita T, Furuichi T, Ito K, Inoue K, Yamana K, Zanma A, Takada K, Ito Y, Komori T.** 2004. Runx2 and Runx3 are essential for chondrocyte maturation, and Runx2 regulates limb growth through induction of Indian hedgehog. Genes Dev **18:**952–963. http://dx.doi.org/10.1101/gad.1174704.
34. **Kronenberg HM.** 2003. Developmental regulation of the growth plate. Nature **423:**332–336. http://dx.doi.org/10.1038/nature01657.
35. **Komori T.** 2005. Regulation of skeletal development by the Runx family of transcription factors. J Cell Biochem **95:**445–453. http://dx.doi.org/10.1002/jcb.20420.
36. **Akiyama H, Kim JE, Nakashima K, Balmes G, Iwai N, Deng JM, Zhang Z, Martin JF, Behringer RR, Nakamura T, de Crombrugghe B.** 2005. Osteo-chondroprogenitor cells are derived from Sox9 expressing precursors. Proc Natl Acad Sci U S A **102:**14665–14670. http://dx.doi.org/10.1073/pnas.0504750102.
37. **Komori T.** 2008. Regulation of bone development and maintenance by Runx2. Front Biosci **13:**898–903. http://dx.doi.org/10.2741/2730.
38. **Levanon D, Negreanu V, Bernstein Y, Bar-Am I, Avivi L, Groner Y.** 1994. AML1, AML2, and AML3, the human members of the runt domain gene-family: cDNA structure, expression, and chromosomal localization. Genomics **23:**425–432. http://dx.doi.org/10.1006/geno.1994.1519.
39. **Devoto M, Shimoya K, Caminis J, Ott J, Tenenhouse A, Whyte MP, Sereda L, Hall S, Considine E, Williams CJ, Tromp G, Kuivaniemi H, Ala-Kokko L, Prockop DJ, Spotila LD.** 1998. First-stage autosomal genome screen in extended pedigrees suggests genes predisposing to low bone mineral density on chromosomes 1p, 2p and 4q. Eur J Hum Genet **6:**151–157. http://dx.doi.org/10.1038/sj.ejhg.5200169.
40. **Devoto M, Specchia C, Li HH, Caminis J, Tenenhouse A, Rodriguez H, Spotila LD.** 2001. Variance component linkage analysis indicates a QTL for femoral neck bone mineral density on chromosome 1p36. Hum Mol Genet **10:**2447–2452. http://dx.doi.org/10.1093/hmg/10.21.2447.
41. **Devoto M, Spotila LD, Stabley DL, Wharton GN, Rydbeck H, Korkko J, Kosich R, Prockop D, Tenenhouse A, Sol-Church K.** 2005. Univariate and bivariate variance component linkage analysis of a whole-genome scan for loci contributing to bone mineral density. Eur J Hum Genet **13:**781–788. http://dx.doi.org/10.1038/sj.ejhg.5201411.
42. **Lee YH, Rho YH, Choi SJ, Ji JD, Song GG.** 2006. Meta-analysis of genome-wide linkage studies for bone mineral density. J Hum Genet **51:**480–486. http://dx.doi.org/10.1007/s10038-006-0390-9.
43. **Xiao P, Shen H, Guo YF, Xiong DH, Liu YZ, Liu YJ, Zhao LJ, Long JR, Guo Y, Recker RR, Deng HW.** 2006. Genomic regions identified for BMD in a large sample including epistatic interactions and gender-specific effects. J Bone Miner Res **21:**1536–1544. http://dx.doi.org/10.1359/jbmr.060717.
44. **Rivadeneira F, Styrkarsdottir U, Estrada K, Halldorsson BV, Hsu YH, Richards JB, Zillikens MC, Kavvoura FK, Amin N, Aulchenko YS, Cupples LA, Deloukas P, Demissie S, Grundberg E, Hofman A, Kong A, Karasik D, van Meurs JB, Oostra B, Pastinen T, Pols HA, Sigurdsson G, Soranzo N, Thorleifsson G, Thorsteinsdottir U, Williams FM, Wilson SG, Zhou Y, Ralston SH, van Duijn CM, Spector T, Kiel DP, Stefansson K, Ioannidis JP, Uitterlinden AG, Genetic Factors for Osteoporosis Consortium.** 2009. Twenty bone-mineral-density loci identified by large-scale meta-analysis of genome-wide association studies. Nat Genet **41:**1199–1206. http://dx.doi.org/10.1038/ng.446.
45. **Estrada K, Styrkarsdottir U, Evangelou E, Hsu YH, Duncan EL, Ntzani EE, Oei L, Albagha OM, Amin N, Kemp JP, Koller DL, Li G, Liu CT, Minster RL, Moayyeri A, Vandenput L, Willner D, Xiao SM, Yerges-Armstrong LM, Zheng HF, Alonso N, Eriksson J, Kammerer CM, Kaptoge SK, Leo PJ, Thorleifsson G, Wilson SG, Wilson JF, Aalto V, Alen M, Aragaki AK, Aspelund T, Center JR, Dailiana Z, Duggan DJ, Garcia M, Garcia-Giralt N, Giroux S, Hallmans G, Hocking LJ, Husted LB, Jameson KA, Khusainova R, Kim GS, Kooperberg C, Koromila T, Kruk M, Laaksonen M, Lacroix AZ, Lee SH, et al.** 2012. Genome-wide meta-analysis identifies 56 bone mineral density loci and reveals 14 loci associated with risk of fracture. Nat Genet **44:**491–501. http://dx.doi.org/10.1038/ng.2249.
46. **Levanon D, Groner Y.** 2009. Runx3-deficient mouse strains circa 2008: resemblance and dissimilarity. Blood Cells Mol Dis **43:**1–5. http://dx.doi.org/10.1016/j.bcmd.2009.01.009.
47. **Dacquin R, Starbuck M, Schinke T, Karsenty G.** 2002. Mouse alpha1(I)-collagen promoter is the best known promoter to drive efficient Cre recombinase expression in osteoblast. Dev Dyn **224:**245–251. http://dx.doi.org/10.1002/dvdy.10100.
48. **Ovchinnikov DA, Deng JM, Ogunrinu G, Behringer RR.** 2000. Col2a1-directed expression of Cre recombinase in differentiating chondrocytes in transgenic mice. Genesis **26:**145–146. http://dx.doi.org/10.1002/(SICI)1526-968X(200002)26:2<145::AID-GENE14>3.0.CO;2-C.
49. **Rodda SJ, McMahon AP.** 2006. Distinct roles for Hedgehog and canon-

ical Wnt signaling in specification, differentiation and maintenance of osteoblast progenitors. Development **133:**3231–3244. http://dx.doi.org/10.1242/dev.02480.
50. **McLeod MJ.** 1980. Differential staining of cartilage and bone in whole mouse fetuses by alcian blue and alizarin red S. Teratology **22:**299–301.
51. **Margolis DS, Kim D, Szivek JA, Lai LW, Lien YH.** 2006. Functionally improved bone in calbindin-D28k knockout mice. Bone **39:**477–484. http://dx.doi.org/10.1016/j.bone.2006.02.064.
52. **Sundin OH, Busse HG, Rogers MB, Gudas LJ, Eichele G.** 1990. Region-specific expression in early chick and mouse embryos of Ghox-lab and Hox 1.6, vertebrate homeobox-containing genes related to Drosophila labial. Development **108:**47–58.
53. **Parfitt AM, Drezner MK, Glorieux FH, Kanis JA, Malluche H, Meunier PJ, Ott SM, Recker RR.** 1987. Bone histomorphometry: standardization of nomenclature, symbols, and units. Report of the ASBMR Histomorphometry Nomenclature Committee. J Bone Miner Res **2:**595–610.
54. **Kajimura D, Lee HW, Riley KJ, Arteaga-Solis E, Ferron M, Zhou B, Clarke CJ, Hannun YA, Depinho RA, Guo EX, Mann JJ, Karsenty G.** 2013. Adiponectin regulates bone mass via opposite central and peripheral mechanisms through FoxO1. Cell Metab **17:**901–915. http://dx.doi.org/10.1016/j.cmet.2013.04.009.
55. **Ducy P, Starbuck M, Priemel M, Shen J, Pinero G, Geoffroy V, Amling M, Karsenty G.** 1999. A Cbfa1-dependent genetic pathway controls bone formation beyond embryonic development. Genes Dev **13:**1025–1036. http://dx.doi.org/10.1101/gad.13.8.1025.
56. **Dresner-Pollak R, Gelb N, Rachmilewitz D, Karmeli F, Weinreb M.** 2004. Interleukin 10-deficient mice develop osteopenia, decreased bone formation, and mechanical fragility of long bones. Gastroenterology **127:**792–801. http://dx.doi.org/10.1053/j.gastro.2004.06.013.
57. **Dumas A, Le Drevo MA, Moreau MF, Guillet C, Basle MF, Chappard D.** 2008. Isolation of osteoprogenitors from murine bone marrow by selection of CD11b negative cells. Cytotechnology **58:**163–171. http://dx.doi.org/10.1007/s10616-009-9184-1.
58. **Callis GM.** 2007. Theory and practice of histological techniques. Churchill Livingstone, New York, NY.
59. **Li B, Boast S, de los Santos K, Schieren I, Quiroz M, Teitelbaum SL, Tondravi MM, Goff SP.** 2000. Mice deficient in Abl are osteoporotic and have defects in osteoblast maturation. Nat Genet **24:**304–308. http://dx.doi.org/10.1038/73542.
60. **Sharma P, Solomon KR, Hauschka PV.** 2006. High-throughput tool for discovery of bone regulating factors. Biotechniques **41:**539–542. http://dx.doi.org/10.2144/000112280.
61. **Irizarry RA, Hobbs B, Collin F, Beazer-Barclay YD, Antonellis KJ, Scherf U, Speed TP.** 2003. Exploration, normalization, and summaries of high density oligonucleotide array probe level data. Biostatistics **4:**249–264. http://dx.doi.org/10.1093/biostatistics/4.2.249.
62. **Corral DA, Amling M, Priemel M, Loyer E, Fuchs S, Ducy P, Baron R, Karsenty G.** 1998. Dissociation between bone resorption and bone formation in osteopenic transgenic mice. Proc Natl Acad Sci U S A **95:**13835–13840. http://dx.doi.org/10.1073/pnas.95.23.13835.
63. **Baker-LePain JC, Nakamura MC, Lane NE.** 2011. Effects of inflammation on bone: an update. Curr Opin Rheumatol **23:**389–395. http://dx.doi.org/10.1097/BOR.0b013e3283474dbe.
64. **Turner CH, Burr DB.** 1993. Basic biomechanical measurements of bone: a tutorial. Bone **14:**595–608. http://dx.doi.org/10.1016/8756-3282(93)90081-K.
65. **Williams SN, Lawrence LA, McDowell LR, Wilkinson NS, Ferguson PW, Warnick AC.** 1991. Criteria to evaluate bone mineralization in cattle. I. Effect of dietary phosphorus on chemical, physical, and mechanical properties. J Anim Sci **69:**1232–1242.
66. **Lefebvre O, Regnier C, Chenard MP, Wendling C, Chambon P, Basset P, Rio MC.** 1995. Developmental expression of mouse stromelysin-3 mRNA. Development **121:**947–955.
67. **Kusano K, Miyaura C, Inada M, Tamura T, Ito A, Nagase H, Kamoi K, Suda T.** 1998. Regulation of matrix metalloproteinases (MMP-2, -3, -9, and -13) by interleukin-1 and interleukin-6 in mouse calvaria: association of MMP induction with bone resorption. Endocrinology **139:**1338–1345. http://dx.doi.org/10.1210/endo.139.3.5818.
68. **Schinke T, Gebauer M, Schilling AF, Lamprianou S, Priemel M, Mueldner C, Neunaber C, Streichert T, Ignatius A, Harroch S, Amling M.** 2008. The protein tyrosine phosphatase Rptpzeta is expressed in differentiated osteoblasts and affects bone formation in mice. Bone **42:**524–534. http://dx.doi.org/10.1016/j.bone.2007.11.009.
69. **Rios HF, Ye L, Dusevich V, Eick D, Bonewald LF, Feng JQ.** 2005. DMP1 is essential for osteocyte formation and function. J Musculoskelet Neuronal Interact **5:**325–327.
70. **Zanotti S, Smerdel-Ramoya A, Canalis E.** 2011. HES1 (hairy and enhancer of split 1) is a determinant of bone mass. J Biol Chem **286:**2648–2657. http://dx.doi.org/10.1074/jbc.M110.183038.
71. **Tu X, Chen J, Lim J, Karner CM, Lee SY, Heisig J, Wiese C, Surendran K, Kopan R, Gessler M, Long F.** 2012. Physiological notch signaling maintains bone homeostasis via RBPjk and Hey upstream of NFATc1. PLoS Genet **8:**e1002577. http://dx.doi.org/10.1371/journal.pgen.1002577.
72. **Horton WA, Hall JG, Hecht JT.** 2007. Achondroplasia. Lancet **370:**162–172. http://dx.doi.org/10.1016/S0140-6736(07)61090-3.
73. **Warshawsky H.** 1982. Embryology and development of the skeletal system, p 33–56. *In* Cruess RL (ed), The musculoskeletal system: embryology, biochemistry and physiology. Churchill Livingstone, New York, NY.
74. **Karsenty G.** 1999. The genetic transformation of bone biology. Genes Dev **13:**3037–3051. http://dx.doi.org/10.1101/gad.13.23.3037.
75. **Klein OF, Carlos AS, Vartanian KA, Chambers VK, Turner EJ, Phillips TJ, Belknap JK, Orwoll ES.** 2001. Confirmation and fine mapping of chromosomal regions influencing peak bone mass in mice. J Bone Miner Res **16:**1953–1961. http://dx.doi.org/10.1359/jbmr.2001.16.11.1953.
76. **Masinde GL, Li X, Gu W, Wergedal J, Mohan S, Baylink DJ.** 2002. Quantitative trait loci for bone density in mice: the genes determining total skeletal density and femur density show little overlap in F2 mice. Calcif Tissue Int **71:**421–428. http://dx.doi.org/10.1007/s00223-001-1113-z.
77. **Spotila LD, Rodriguez H, Koch M, Adams K, Caminis J, Tenenhouse HS, Tenenhouse A.** 2000. Association of a polymorphism in the TNFR2 gene with low bone mineral density. J Bone Miner Res **15:**1376–1383. http://dx.doi.org/10.1359/jbmr.2000.15.7.1376.
78. **Kajita M, Ezura Y, Iwasaki H, Ishida R, Yoshida H, Kodaira M, Suzuki T, Hosoi T, Inoue S, Shiraki M, Orimo H, Emi M.** 2003. Association of the −381T/C promoter variation of the brain natriuretic peptide gene with low bone-mineral density and rapid postmenopausal bone loss. J Hum Genet **48:**77–81. http://dx.doi.org/10.1007/s100380300010.
79. **McLean RR, Karasik D, Selhub J, Tucker KL, Ordovas JM, Russo GT, Cupples LA, Jacques PF, Kiel DP.** 2004. Association of a common polymorphism in the methylenetetrahydrofolate reductase (MTHFR) gene with bone phenotypes depends on plasma folate status. J Bone Miner Res **19:**410–418. http://dx.doi.org/10.1359/JBMR.0301261.
80. **Huang QY, Li GH, Kung AW.** 2009. Multiple osteoporosis susceptibility genes on chromosome 1p36 in Chinese. Bone **44:**984–988. http://dx.doi.org/10.1016/j.bone.2009.01.368.
81. **Stricker S, Fundele R, Vortkamp A, Mundlos S.** 2002. Role of Runx genes in chondrocyte differentiation. Dev Biol **245:**95–108. http://dx.doi.org/10.1006/dbio.2002.0640.
82. **Johnson K, Zhu S, Tremblay MS, Payette JN, Wang J, Bouchez LC, Meeusen S, Althage A, Cho CY, Wu X, Schultz PG.** 2012. A stem cell-based approach to cartilage repair. Science **336:**717–721. http://dx.doi.org/10.1126/science.1215157.